Entanglement-Assisted Communication Surpassing the Ultimate Classical Capacity

Shuhong Hao, Haowei Shi, Wei Li, Igffrey H. Shapiro, Quntao Zhuang, 4.2 and Zheshen Zhang, Identification of Materials Science and Engineering, University of Arizona, Tucson, Arizona 85721, USA

James C. Wyant College of Optical Sciences, University of Arizona, Tucson, Arizona 85721, USA

Research Laboratory of Electronics, Massachusetts Institute of Technology, Cambridge, Massachusetts 02139, USA

Department of Electrical and Computer Engineering, University of Arizona, Tucson, Arizona 85721, USA

(Received 17 November 2020; accepted 17 May 2021; published 22 June 2021)

Entanglement underpins a variety of quantum-enhanced communication, sensing, and computing capabilities. Entanglement-assisted communication (EACOMM) leverages entanglement preshared by communicating parties to boost the rate of classical information transmission. Pioneering theory works showed that EACOMM can enable a communication rate well beyond the ultimate classical capacity of optical communications, but an experimental demonstration of any EACOMM advantage remains elusive. In this Letter we report the implementation of EACOMM surpassing the classical capacity over lossy and noisy bosonic channels. We construct a high-efficiency entanglement source and a phase-conjugate quantum receiver to reap the benefit of preshared entanglement, despite entanglement being broken by channel loss and noise. We show that EACOMM beats the Holevo-Schumacher-Westmoreland capacity of classical communication by up to 16.3%, when both protocols are subject to the same power constraint at the transmitter. As a practical performance benchmark, we implement a classical communication protocol with the identical characteristics for the encoded signal, showing that EACOMM can reduce the bit-error rate by up to 69% over the same bosonic channel. Our work opens a route to provable quantum advantages in a wide range of quantum information processing tasks.

DOI: 10.1103/PhysRevLett.126.250501

Introduction.—Entanglement is the cornerstone for a wide range of quantum information processing applications including quantum-secured communication [1], quantumenhanced sensing [2], and quantum computing [3]. In addition, entanglement preshared by communicating parties can increase the reliable transmission rate of classical information, a paradigm known as entanglementassisted (EA) communication (EACOMM) [4-11]. The pioneering work by Bennett, Shor, Smolin, and Thapliyal [5] showed that the channel capacity with EA surpasses the ultimate classical capacity without EA, i.e., the Holevo-Schumacher-Westmoreland (HSW) capacity [12–14]. Surprisingly, for lossy and noisy bosonic channels, which are ubiquitous in optical and microwave communications, photonic sensing, and one-way quantum computing [15], the ratio between the EA capacity and the HSW capacity can diverge. Notably, the EA-capacity advantage persists even when a lossy and noisy channel breaks the initial preshared entanglement.

This seminal EA-capacity result, albeit encouraging, does not elucidate an EACOMM protocol to reap the promised advantage. In this regard, superdense coding is a well-studied EACOMM scenario that leverages stronger-than-classical correlations between entangled photons to encode more than one classical bit of information on each transmitted photon [16,17]. However, EACOMM experiments [18–25] based on the polarization, temporal, and

path degrees of freedom have dismissed the phase correlations embedded in entangled bosonic modes, thereby making them unable to beat the HSW capacity (Supplemental Material [26]). Studies of EACOMM protocols over bosonic channels encompassed continuousvariable superdense coding [31–33] and mode permutation or selection encoding [11,34–36]. Unfortunately, the former failed to surpass the HSW capacity due to poor performance in the presence of channel loss and noise [37–40], whereas the latter requires large-volume quantum memories that are not yet available. Recently, Shi et al. [41] formulated a theoretical framework to devise the optimal entangled state and encoding format suitable for loss and noise resilient EACOMM. That theory work also proposed practical quantum receiver structures to enable an EACOMM rate superior to the HSW capacity.

In this Letter, we report an EACOMM experiment over lossy and noisy bosonic channels at communication rates up to 16.3%±4.1% above the HSW capacity. In contrast to many superdense coding protocols that resort to the probabilistic arrival of single photons at the receiver due to channel loss, our EACOMM protocol harnesses the phase correlations between entangled bosonic modes so that all transmitted bits are decoded. A low-gain quantum phase-conjugate receiver (PCR) is constructed to extract phase correlations while reducing the impact of noise power. Apart from benchmarking against the ultimate

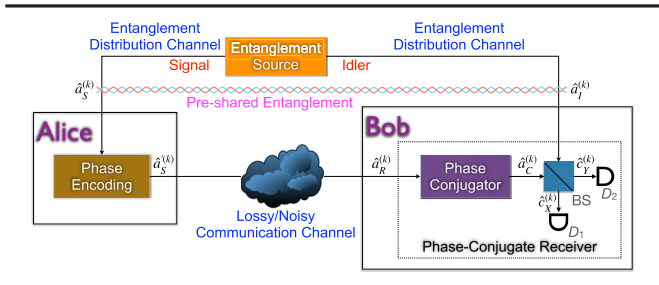


FIG. 1. Schematic of the EACOMM protocol. An entanglement source distributes two-mode squeezed vacuum signal-idler pairs $\{\hat{a}_S^{(k)}, \hat{a}_I^{(k)}\}$ to Alice and Bob. Alice phase encodes on $\hat{a}_S^{(k)}$ and transmits the encoded modes $\hat{a}_S^{\prime(k)}$ to Bob through a lossy and noisy channel. Bob produces $\hat{a}_C^{(k)}$ by phase conjugating the received modes $\hat{a}_R^{(k)}$. $\hat{a}_C^{(k)}$ and $\hat{a}_I^{(k)}$ interfere on a balanced beam splitter (BS), whose outputs undergo photon counting by photodetectors D_1 and D_2 to derive the difference photon number, from which Alice's encoded classical bit is inferred. See text for details of the evolution of the mode operators.

HSW capacity, we show that EACOMM achieves error probabilities up to 69% lower than what a practical classical communication (CCOMM) system can afford. Our work achieves a provable quantum advantage and would create new opportunities for entanglement-enhanced quantum information processing.

Protocol.—The schematic for the implemented EACOMM protocol is sketched in Fig. 1. Key components include (1) an entanglement source; (2) two low-loss entanglement distribution channels connecting the source to Alice and Bob; (3) phase encoding on Alice's share of the entanglement, i.e., the signal; and (4) a PCR that Bob operates to perform a joint measurement on the received signal from a lossy and noisy channel and Bob's share of the entanglement, i.e., the idler.

Prior to transmitting one bit of classical information, the entanglement source emits M independent and identically distributed two-mode squeezed vacuum (TMSV) signal-idler mode pairs, described by annihilation operators $\{\hat{a}_{S}^{(k)},\hat{a}_{I}^{(k)}\}_{k=1}^{M},$ and sends the signal modes to Alice and the idler modes to Bob through two low-loss, noiseless entanglement-distribution channels. The mean photon number of a signal or an idler mode is $\langle \hat{a}_S^{\dagger(k)} \hat{a}_S^{(k)} \rangle = \langle \hat{a}_I^{\dagger(k)} \hat{a}_I^{(k)} \rangle = N_S$. To encode a classical bit $b \in \{0,1\}$, Alice applies binary phase-shift keying on all M signal modes, yielding encoded signal modes $\{\hat{a}_S^{\prime(k)}=(-1)^b\hat{a}_S^{(k)}\}_{k=1}^M$ that are subsequently transmitted to Bob through a bosonic thermal-loss channel [42], \mathcal{L}^{κ,N_B} , characterized by its transmissivity κ and its noise's per-mode average photon number N_B . The noise photons are effectively introduced by thermal background modes $\{\hat{a}_{B}^{(k)}\}_{k=1}^{M}$, each with a mean photon number of $\langle \hat{a}_B^{\dagger(k)} \hat{a}_B^{(k)} \rangle = N_B/(1-\kappa)$. The mode evolution relation in the Heisenberg picture gives Bob's received signal modes $\{\hat{a}_R^{(k)} = \sqrt{\kappa}\hat{a}_S^{\prime(k)} + \sqrt{1-\kappa}\hat{a}_B^{(k)}\}_{k=1}^M$ that contain N_B thermal noise photons per mode on average. Both the employed TMSV state and phase encoding have been proven optimum for EACOMM [41].

To decode the classical bit, Bob uses a PCR to perform a joint measurement on the received signal modes $\{\hat{a}_{R}^{(k)}\}_{k=1}^{M}$ and idler modes $\{\hat{a}_{I}^{(k)}\}_{k=1}^{M}$ from the entanglement source [43]. In the PCR, phase-conjugate modes, $\hat{a}_C^{(k)}$, of the received signal are obtained in a parametric process with gain G, viz. $\{\hat{a}_C^{(k)} = \sqrt{G}\hat{a}_v^{(k)} + \sqrt{G-1}\hat{a}_R^{\dagger(k)}\}_{k=1}^M$, where $\{\hat{a}_v^{(k)}\}_{k=1}^M$ are vacuum-state modes. The phase-conjugate modes then interfere with the idler modes on a balanced beam splitter, leading to the modes $\{\hat{c}_X^{(k)} =$ $(\hat{a}_C^{(k)} + \hat{a}_I^{(k)})/\sqrt{2}\}_{k=1}^M$ and $\{\hat{c}_Y^{(k)} = (\hat{a}_I^{(k)} - \hat{a}_C^{(k)})/\sqrt{2}\}_{k=1}^M$ at the two output ports. Photon counting at each output port measures M modes simultaneously, so the two detectors generate two jointly Gaussian variables N_X , N_Y in the asymptotic limit of $M \gg 1$. The difference photon number, defined as $N \equiv N_X - N_Y$, is dependent on the phase-insensitive cross correlations $\{\langle \hat{a}_C^{\dagger(k)} \hat{a}_I^{(k)} \rangle\}_{k=1}^M$, which stem from the phase-sensitive cross correlations $\{\langle \hat{a}_S^{(k)} \hat{a}_I^{(k)} \rangle\}_{k=1}^M$ of the TMSV states. The decoded classical bit \tilde{b} is set to 0 (1) when $N \ge 0$ (N < 0). The bit-error rate (BER) of EACOMM using TMSV states and the PCR can be analytically derived as [41]

$$P_e = \frac{1}{2} \operatorname{erfc}\left(\sqrt{\frac{2M\eta_D \kappa_I \kappa N_S (N_S + 1)}{N_B (1 + 2\delta \eta + 2\eta_D \kappa_I N_S)}}\right), \quad (1)$$

in the $N_B\gg 1$, $M\gg 1$ limit (see Supplemental Material [26] for the full formula), where η_D is the effective detection efficiency, κ_I is the idler's overall efficiency including the source and entanglement-distribution efficiencies, and $\delta\eta$ models deviation of the BS transmissivity from 50%.

With equal probability of Alice sending 0s and 1s, the BER then determines the mutual information between Alice and Bob, obtained by transmitting M modes, as

$$I(A;B) = 1 + P_e \log_2(P_e) + (1 - P_e) \log_2(1 - P_e).$$
 (2)

Without EA, the HSW capacity per mode, subject to the same mean photon-number constraint N_S , has been derived as [44]

$$C(\mathcal{L}^{\kappa,N_B}) = g(\kappa N_S + N_B) - g(N_B), \tag{3}$$

where $g(N) = (N+1)\log_2(N+1) - N\log_2(N)$ is the von Neumann entropy of a thermal state with mean photon number N. Demonstrating $I(A;B) > MC(\mathcal{L}^{\kappa,N_B})$ will prove that EACOMM surpasses the ultimate classical capacity.

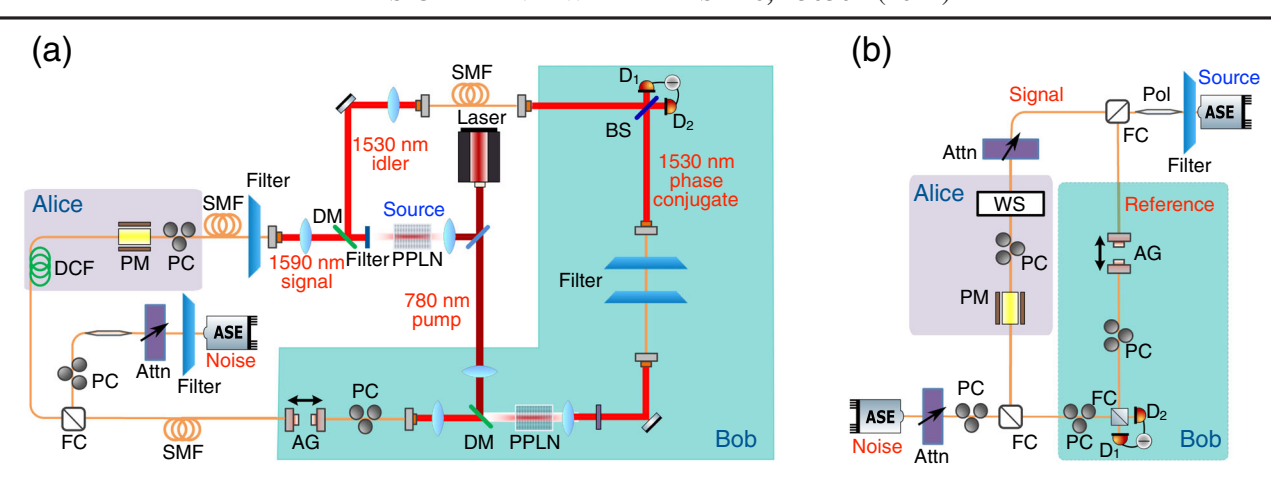


FIG. 2. Experimental diagrams for (a) EACOMM and (b) CCOMM. AG, air gap; ASE, amplified spontaneous emission; Attn, attenuator; BS, beam splitter; *D*, detector; DCF, dispersion compensating fiber; DM, dichroic mirror; FC, fiber coupler; PC, polarization controller; PM, phase modulator; Pol, polarizer; PPLN, periodically poled lithium niobate; SMF, single-mode fiber; WS, wave shaper.

Experimental setup.—The experimental diagram for EACOMM is depicted in Fig. 2(a). The entanglement source comprises a periodically poled lithium niobate (PPLN) crystal pumped by a 780-nm laser to produce broadband spontaneous parametric down conversion photons centered at 1560 nm. In the experiment, we pick the signal and idler modes to situate, respectively, around 1590 nm and 1530 nm. Because of energy conservation in down conversion, the signal and idler form entangled mode pairs each described by a TMSV state. A dichroic mirror separates the signal and idler modes. The signal and idler are subsequently coupled into single-mode fibers through two collimators. A flat-top optical filter is then applied on the signal to carve out a 16-nm band centered on 1590 nm, corresponding to an optical bandwidth of $W \sim 2$ THz. The signal photons are distributed to Alice while the idler photons are sent to Bob through two entanglement distribution channels consisting of low-loss single-mode fibers. The overall efficiency κ_I for the idler distribution and storage is measured to be 96%.

To encode a classical bit b at Alice's transmitter, an electro-optic modulator driven by a BER tester imparts a T-second-long phase shift of $b\pi$ on M=WT signal modes. The phase-modulated signal modes are sent to Bob through an optical fiber link. An L-band amplified spontaneous emission (ASE) source, filtered to a 16-nm band centered on 1590 nm, serves as the thermal light source due to its second-order coherence property [45] and multimode photon statistics [46]. The ASE light is combined with the encoded signal on a fiber coupler. We construct a free-space air gap to fine tune the relative delay between the signal and idler photons so that they arrive simultaneously at the PCR.

At Bob's terminal, we couple the signal photons from fiber to free space via a collimator. The signal is then sent to a second PPLN crystal pumped by a 780-nm laser to generate the phase-conjugate modes at the idler wavelength of

1530 nm via a difference-frequency generation process with gain $G = 1 + 0.257 \times 10^{-3}$. The output of the PPLN crystal is coupled back to optical fiber via a collimator. Two cascaded bandpass filters then reject the signal photons at 1590 nm, and the remaining phase-conjugate photons are coupled back to free space. The phase-conjugate photons interfere with the idler photons on a 50:50 beam splitter whose $\delta \eta \sim 10^{-3}$. The photons at the two output ports of the beam splitter are diverted to a balanced detector with an effective detection efficiency of $\eta_D = 95\%$, which includes the 99% quantum efficiency of the photodiodes and the interference visibility of 98%. Note that the measurement is not based on either coincidence counting or Hong-Ou-Mandel interference because at the receiver the noise photons are more than 8 orders of magnitude brighter than the photons originating from the source. The output electrical signal from the detector is directed to the BER tester.

Demonstrating quantum advantages.—We first demonstrate that EACOMM over lossy and noisy channels can achieve a rate higher than any CCOMM protocol without EA can afford, thereby proving EACOMM's quantum advantage. In the experiment, the power of the transmitted signal is fixed at $P_S = 195 \text{ pW}$ so that $N_S = P_S/\hbar\omega_0 W = 7.8 \times 10^{-4}$, where \hbar is the reduced Planck constant, and ω_0 is the frequency of the signal photons. In measuring the BERs, N_B is tuned from 10^4 to 10⁵ by increasing the output power of the ASE source. The corresponding mutual information given by Eq. (2) is plotted alongside the HSW capacity and the EA capacity (Supplemental Material [26]) in Fig. 3, showing experimental EACOMM's advantages at $N_B > 5 \times 10^4$. As we see, the theory (blue curve) agrees well with the experimental results (blue dots); the disadvantage at low N_B is due to effects from additional loss in the receiver (Supplemental Material [26]). This result indicates that the EACOMM's advantage becomes even more pronounced over a more noisy channel.

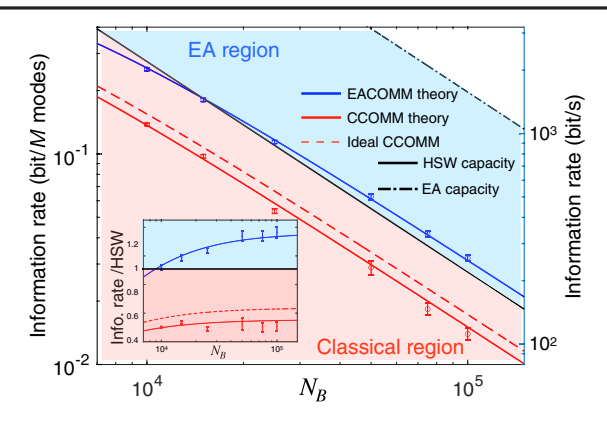


FIG. 3. The information rates for EACOMM (blue), practical CCOMM (red), the classical capacity (black solid), and the EA capacity (black dash-dotted) at different thermal background noise levels. Curves, theory; dots, experimental data. (Inset) EACOMM rate over the HSW capacity (blue) and the practical CCOMM rate over the HSW capacity (red). EACOMM information rate $(0.0320 \pm 0.0011 \text{ bit}/M \text{ modes})$ surpasses HSW capacity (0.0275 bit/M modes) by more than 4 standard deviations at $N_B = 10^5$. Red dashed curves, theory for ideal CCOMM with $\kappa_F = 1$; blue shaded area, EA region; red shaded area, classical region. Error bars for EACOMM (CCOMM) are derived from 50 (15) consecutive BER measurements each using 10^4 bits. In the experiment, $\kappa = 0.014$, $M = 2.5 \times 10^8$, $\kappa_I = 0.96$, $\eta_D = 0.95$, $\delta \eta = 10^{-3}$, $N_S = 7.8 \times 10^{-4}$, and $N_R = 1.2 \times 10^3$.

Given the optical bandwidth W and the source brightness $N_{\rm S}$, the HSW capacity sets an ultimate limit for the communication rate without EA. In practice, however, approaching the classical capacity would require the optimal encoding and the optimum joint-detection receiver for that encoding, which are beyond the reach of current technology. To experimentally assess how practical CCOMM without EA performs, we implement a protocol based on broadband light and multimode encoding and measurements, as illustrated in Fig. 2(b). Broadband light was previously utilized by floodlight quantum key distribution to boost secret-key rates [47–49]. The CCOMM protocol's encoded signal shares the same characteristics, including the power, encoding rate, and format as that in the EACOMM protocol (Supplemental Material [26]). In the CCOMM experiment, ASE light is filtered to 16-nm bandwidth and then split into two arms that differ substantially in their optical powers. The weak output arm with a per-mode mean photon number $N_S \ll 1$ serves as the signal and is distributed to Alice, whereas the strong output arm with a per-mode mean photon number $N_R \gg 1$ becomes a broadband reference and is sent to Bob. From Alice's perspective, her received quantum states are identical to her share of the entangled state in EACOMM. As such, we make use of the same phasemodulation scheme to encode classical bits that EACOMM does. At Bob's terminal, the received signal and the reference interfere on a 50:50 fiber coupler, whose two outputs are measured by a balanced detector that produces a difference photocurrent. Like the EACOMM experiment, a phase-locking servo loop is implemented to ensure stable BER measurements. Given $N_R \gg 1$ and $N_B \gg N_S$, the error rate of the broadband light homodyne detection approaches that for homodyne detection of coherent states (Supplemental Material [26])

$$P_e = \frac{1}{2} \operatorname{erfc}\left(\sqrt{\frac{M\kappa\kappa_F N_S}{N_B + 1/2}}\right),\tag{4}$$

where $\kappa_F = 0.87$ is a fitting parameter accounting for experimental nonidealities including imperfect dispersion matching between the signal and the reference and detector balancing.

The performance of EACOMM is compared with that of CCOMM under three parameter settings. First, the BERs of the CCOMM protocol under different amounts of channel background thermal noise are measured. The corresponding information rates are plotted in Fig. 3, showing good agreement with the theoretical model. EACOMM enjoys an up to 126% information-rate advantage over the CCOMM protocol. We then measure the BERs of the EACOMM and CCOMM protocols at different number of modes per encoding, i.e., the encoding rate, and plot the experimental data in Fig. 4(a), showing a substantial BER advantage for EACOMM over CCOMM. Figure 4(b) plots the BER data vs source brightness N_S . EACOMM demonstrates a reduced BER at all N_S levels, with the largest BER reduction of 40% measured at $N_S = 7.8 \times 10^{-4}$.

Discussion.—EACOMM uses preshared entanglement to improve the rates of transferring classical information, instead of quantum bits [50]. While the current experiment emulates bright background noise injection at the telecommunication wavelength, our model also applies to distributing the preshared entanglement at optical wavelengths [51] and then wavelength converting [52] the signal photons to support EACOMM in the microwave [53] or covert communication in the long-wave infrared region [54]. In a future dynamic operational environment, entanglement, as a quantum resource, will be preloaded into local quantum memories when reliable entanglement distribution channels are available and will be subsequently retrieved, on demand, to boost the communication rate when only lossy and noisy channels are accessible.

Quantum illumination (QI) [55] uses entanglement over lossy and noisy bosonic channels to detect the presence of a target [56–60] or to defeat a passive eavesdropper [61–63]. Were QI secure communication to use an optical amplifier in its entanglement sharing, it would break the entanglement before sending the encoded signal and thus forfeit the benefit of EACOMM. Also, the optical parametric amplifier receiver used in the previous QI experiments introduces additional loss on the idler beam such that EACOMM's

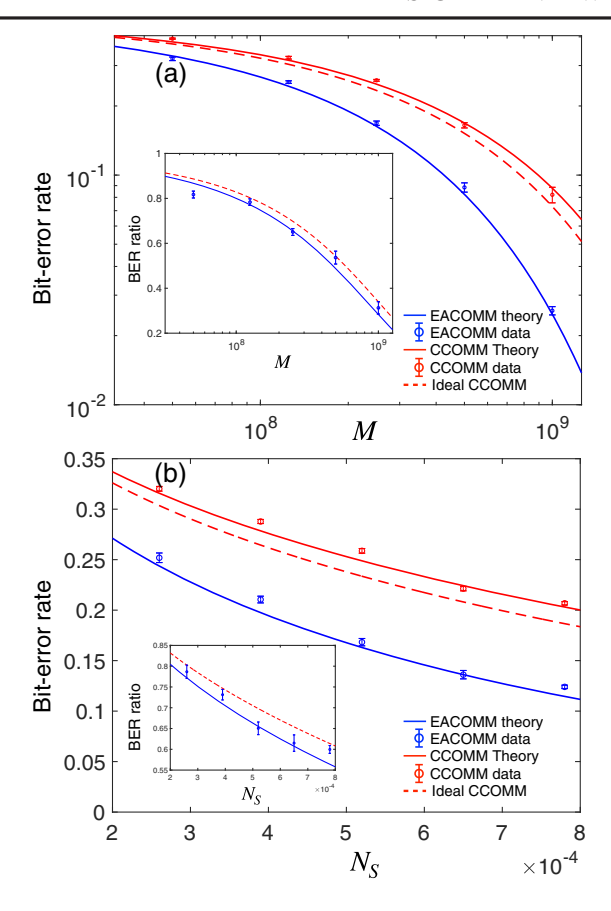


FIG. 4. (a) Bit-error rate vs number of modes per encoding M. In the measurements, $\kappa = 0.043$, $N_B = 2.1 \times 10^4$, and $N_S = 5.2 \times 10^{-4}$. (b) Bit-error rate vs source brightness N_S . In the measurements, $\kappa = 0.043$, $M = 2.5 \times 10^8$, $N_R = 1.2 \times 10^3$, and $N_B = 2.1 \times 10^4$. (Insets) BER ratio between EACOMM and CCOMM. Dots, experimental data; curves, theory; dashed curves, ideal CCOMM with $\kappa_F = 1$. Error bars are derived from 15 consecutive BER measurements each based on 10^4 bits.

stringent requirements on the efficiency of the quantum receiver cannot be satisfied. The PCR, in contrast, first generates a bright phase-conjugate beam so that any additional loss has minimal effect on the receiver performance. Hence, the PCR is able to attain a large EACOMM advantage sufficient to outperform the classical capacity. Notably, the EACOMM advantage can be extended and generalized to a scenario without a phase reference [64] and a quantum network with multiaccess channels [65]. In state-of-the-art optical communication systems, the PCR can be implemented in silicon photonics chips by leveraging the four-wave mixing process in silicon or silicon nitride.

Although we have demonstrated EACOMM's surpassing the HSW capacity, the PCR does not saturate the EA capacity. A recent study proposed a quantum-receiver structure based on single-photon-level sum-frequency generation [66] and multimode interference to achieve the $\log_2(N_S)$ scaling of EACOMM [67], thereby pointing to a

promising route toward realizing a larger EACOMM advantage over CCOMM.

Conclusions.—We have developed an efficient entanglement source and quantum receiver to demonstrate EACOMM beyond the classical capacity. Our work demonstrates the power of preshared entanglement in enhancing the rate of transmitting classical information over lossy and noisy bosonic channels. This result would pave a new avenue toward utilizing entanglement to achieve a provable quantum advantage in applications involving substantial loss and noise, such as low probability of intercept [54,68], covert sensing [69], and noninvasive imaging [70].

We gratefully acknowledge funding support by the National Science Foundation Grants No. CCF-1907918, No. ECCS-1828132, and No. EEC-1941583 and General Dynamics Mission Systems. Q. Z. also acknowledges support from Defense Advanced Research Projects Agency (DARPA) under Young Faculty Award (YFA) Grant No. N660012014029. J. H. S. acknowledges support from the MITRE Corporation's Quantum Moonshot Program. The authors thank HC Photonics for providing the nonlinear crystals and William Clark and Saikat Guha for helpful discussions.

- zsz@arizona.edu
- [1] A. K. Ekert, Quantum Cryptography Based on Bell's Theorem, Phys. Rev. Lett. 67, 661 (1991).
- [2] V. Giovannetti, S. Lloyd, and L. Maccone, Quantumenhanced positioning and clock synchronization, Nature (London) 412, 417 (2001).
- [3] P. W. Shor, Polynomial-time algorithms for prime factorization and discrete logarithms on a quantum computer, SIAM Rev. 41, 303 (1999).
- [4] C. H. Bennett, P. W. Shor, J. A. Smolin, and A. V. Thapliyal, Entanglement-Assisted Classical Capacity of Noisy Quantum Channels, Phys. Rev. Lett. **83**, 3081 (1999).
- [5] C. H. Bennett, P. W. Shor, J. A. Smolin, and A. V. Thapliyal, Entanglement-assisted capacity of a quantum channel and the reverse Shannon theorem, IEEE Trans. Inf. Theory 48, 2637 (2002).
- [6] A. S. Holevo, On entanglement-assisted classical capacity, J. Math. Phys. (N.Y.) 43, 4326 (2002).
- [7] P. W. Shor, The classical capacity achievable by a quantum channel assisted by limited entanglement, arXiv:quant-ph/0402129.
- [8] M.-H. Hsieh, I. Devetak, and A. Winter, Entanglement-assisted capacity of quantum multiple-access channels, IEEE Trans. Inf. Theory **54**, 3078 (2008).
- [9] Q. Zhuang, E. Y. Zhu, and P. W. Shor, Additive Classical Capacity of Quantum Channels Assisted by Noisy Entanglement, Phys. Rev. Lett. 118, 200503 (2017).
- [10] M. M. Wilde and M.-H. Hsieh, The quantum dynamic capacity formula of a quantum channel, Quantum Inf. Process. 11, 1431 (2012).

- [11] M. M. Wilde, P. Hayden, and S. Guha, Information Trade-Offs for Optical Quantum Communication, Phys. Rev. Lett. 108, 140501 (2012).
- [12] P. Hausladen, R. Jozsa, B. Schumacher, M. Westmoreland, and W. K. Wootters, Classical information capacity of a quantum channel, Phys. Rev. A 54, 1869 (1996).
- [13] B. Schumacher and M. D. Westmoreland, Sending classical information via noisy quantum channels, Phys. Rev. A 56, 131 (1997).
- [14] A. S. Holevo, The capacity of the quantum channel with general signal states, IEEE Trans. Inf. Theory 44, 269 (1998).
- [15] N. C. Menicucci, P. Van Loock, M. Gu, C. Weedbrook, T. C. Ralph, and M. A. Nielsen, Universal Quantum Computation with Continuous-Variable Cluster States, Phys. Rev. Lett. 97, 110501 (2006).
- [16] C. H. Bennett and S. J. Wiesner, Communication Via Oneand Two-Particle Operators on Einstein-Podolsky-Rosen States, Phys. Rev. Lett. 69, 2881 (1992).
- [17] Y. Guo, B.-H. Liu, C.-F. Li, and G.-C. Guo, Advances in quantum dense coding, Adv. Quantum Technol. 2, 1900011 (2019).
- [18] K. Mattle, H. Weinfurter, P. G. Kwiat, and A. Zeilinger, Dense Coding in Experimental Quantum Communication, Phys. Rev. Lett. 76, 4656 (1996).
- [19] J. T. Barreiro, T.-C. Wei, and P. G. Kwiat, Beating the channel capacity limit for linear photonic superdense coding, Nat. Phys. 4, 282 (2008).
- [20] T. Schaetz, M. D. Barrett, D. Leibfried, J. Chiaverini, J. Britton, W. M. Itano, J. D. Jost, C. Langer, and D. J. Wineland, Quantum Dense Coding with Atomic Qubits, Phys. Rev. Lett. 93, 040505 (2004).
- [21] R. Prevedel, Y. Lu, W. Matthews, R. Kaltenbaek, and K. J. Resch, Entanglement-Enhanced Classical Communication Over a Noisy Classical Channel, Phys. Rev. Lett. 106, 110505 (2011).
- [22] A. Chiuri, S. Giacomini, C. Macchiavello, and P. Mataloni, Experimental achievement of the entanglement-assisted capacity for the depolarizing channel, Phys. Rev. A 87, 022333 (2013).
- [23] B. P. Williams, R. J. Sadlier, and T. S. Humble, Superdense Coding Over Optical Fiber Links with Complete Bell-State Measurements, Phys. Rev. Lett. **118**, 050501 (2017).
- [24] B.-H. Liu, X.-M. Hu, Y.-F. Huang, C.-F. Li, G.-C. Guo, A. Karlsson, E.-M. Laine, S. Maniscalco, C. Macchiavello, and J. Piilo, Efficient superdense coding in the presence of non-Markovian noise, Europhys. Lett. 114, 10005 (2016).
- [25] X.-M. Hu, Y. Guo, B.-H. Liu, Y.-F. Huang, C.-F. Li, and G.-C. Guo, Beating the channel capacity limit for superdense coding with entangled ququarts, Sci. Adv. 4, eaat9304 (2018).
- [26] See Supplemental Material at http://link.aps.org/supplemental/ 10.1103/PhysRevLett.126.250501 for a detailed description for the experiment setups and the theoretical models, which includes Refs. [27–30].
- [27] R. S. Bennink, Optimal collinear Gaussian beams for spontaneous parametric down-conversion, Phys. Rev. A 81, 053805 (2010).
- [28] P. B. Dixon, D. Rosenberg, V. Stelmakh, M. E. Grein, R. S. Bennink, E. A. Dauler, A. J. Kerman, R. J. Molnar, and

- F. N. C. Wong, Heralding efficiency and correlated-mode coupling of near-IR fiber-coupled photon pairs, Phys. Rev. A **90**, 043804 (2014).
- [29] J. D. Franson, Nonlocal cancellation of dispersion, Phys. Rev. A 45, 3126 (1992).
- [30] J. H. Shapiro, Dispersion cancellation with phase-sensitive Gaussian-state light, Phys. Rev. A 81, 023824 (2010).
- [31] M. Ban, Quantum dense coding via a two-mode squeezed-vacuum state, J. Opt. B: Quantum Semiclassical Opt. 1, L9 (1999).
- [32] S. L. Braunstein and H. J. Kimble, Dense coding for continuous variables, Phys. Rev. A 61, 042302 (2000).
- [33] M. Ban, Quantum dense coding of continuous variables in a noisy quantum channel, J. Opt. B: Quantum Semiclass. Opt. 2, 786 (2000).
- [34] A. Anshu, R. Jain, and N. A. Warsi, Building blocks for communication over noisy quantum networks, IEEE Trans. Inf. Theory **65**, 1287 (2019).
- [35] H. Qi, Q. Wang, and M. M. Wilde, Applications of position-based coding to classical communication over quantum channels, J. Phys. A 51, 444002 (2018).
- [36] S. Khabbazi Oskouei, S. Mancini, and M. M. Wilde, Union bound for quantum information processing, Proc. R. Soc. 475, 20180612 (2019).
- [37] M. Sohma and O. Hirota, Capacity of a channel assisted by two-mode squeezed states, Phys. Rev. A 68, 022303 (2003).
- [38] J. Mizuno, K. Wakui, A. Furusawa, and M. Sasaki, Experimental demonstration of entanglement-assisted coding using a two-mode squeezed vacuum state, Phys. Rev. A 71, 012304 (2005).
- [39] S. Barzanjeh, S. Pirandola, and C. Weedbrook, Continuous-variable dense coding by optomechanical cavities, Phys. Rev. A **88**, 042331 (2013).
- [40] X. Li, Q. Pan, J. Jing, J. Zhang, C. Xie, and K. Peng, Quantum Dense Coding Exploiting a Bright Einstein-Podolsky-Rosen Beam, Phys. Rev. Lett. 88, 047904 (2002).
- [41] H. Shi, Z. Zhang, and Q. Zhuang, Practical Route to Entanglement-Assisted Communication Over Noisy Bosonic Channels, Phys. Rev. Applied 13, 034029 (2020).
- [42] C. Weedbrook, S. Pirandola, R. García-Patrón, N. J. Cerf, T. C. Ralph, J. H. Shapiro, and S. Lloyd, Gaussian quantum information, Rev. Mod. Phys. 84, 621 (2012).
- [43] S. Guha and B. I. Erkmen, Gaussian-state quantumillumination receivers for target detection, Phys. Rev. A 80, 052310 (2009).
- [44] V. Giovannetti, R. García-Patrón, N. J. Cerf, and A. S. Holevo, Ultimate classical communication rates of quantum optical channels, Nat. Photonics **8**, 796 (2014).
- [45] I. V. Doronin, E. S. Andrianov, A. A. Zyablovsky, A. A. Pukhov, Y. E. Lozovik, A. P. Vinogradov, and A. A. Lisyansky, Second-order coherence properties of amplified spontaneous emission, Opt. Express 27, 10991 (2019).
- [46] W. S. Wong, H. A. Haus, L. A. Jiang, P. B. Hansen, and M. Margalit, Photon statistics of amplified spontaneous emission noise in a 10-Gbit/s optically preamplified directdetection receiver, Opt. Lett. 23, 1832 (1998).
- [47] Q. Zhuang, Z. Zhang, J. Dove, F. N. C. Wong, and J. H. Shapiro, Floodlight quantum key distribution: A practical route to gigabit-per-second secret-key rates, Phys. Rev. A 94, 012322 (2016).

- [48] Z. Zhang, Q. Zhuang, F. N. C. Wong, and J. H. Shapiro, Floodlight quantum key distribution: Demonstrating a framework for high-rate secure communication, Phys. Rev. A 95, 012332 (2017).
- [49] Z. Zhang, C. Chen, Q. Zhuang, F. N. C. Wong, and J. H. Shapiro, Experimental quantum key distribution at 1.3 gigabit-per-second secret-key rate over a 10 dB loss channel, Quantum Sci. Technol. 3, 025007 (2018).
- [50] Á. Cuevas, M. Proietti, M. A. Ciampini, S. Duranti, P. Mataloni, M. F. Sacchi, and C. Macchiavello, Experimental Detection of Quantum Channel Capacities, Phys. Rev. Lett. 119, 100502 (2017).
- [51] J. Yin, Y. Cao, Y.-H. Li, S.-K. Liao, L. Zhang, J.-G. Ren, W.-Q. Cai, W.-Y. Liu, B. Li, H. Dai *et al.*, Satellite-based entanglement distribution over 1200 kilometers, Science 356, 1140 (2017).
- [52] N. J. Lambert, A. Rueda, F. Sedlmeir, and H. G. Schwefel, Coherent conversion between microwave and optical photons—an overview of physical implementations, Adv. Quantum Technol. 3, 1900077 (2020).
- [53] Y. Ding, J. Zhang, and V. Fusco, Frequency diverse array ofdm transmitter for secure wireless communication, Electron. Lett. 51, 1374 (2015).
- [54] B. A. Bash, A. H. Gheorghe, M. Patel, J. L. Habif, D. Goeckel, D. Towsley, and S. Guha, Quantum-secure covert communication on bosonic channels, Nat. Commun. 6, 8626 (2015).
- [55] J. H. Shapiro, The quantum illumination story, IEEE Aerospace and Electronics Systems Magazine 35, 8 (2020).
- [56] S.-H. Tan, B. I. Erkmen, V. Giovannetti, S. Guha, S. Lloyd, L. Maccone, S. Pirandola, and J. H. Shapiro, Quantum Illumination with Gaussian States, Phys. Rev. Lett. 101, 253601 (2008).
- [57] S. Barzanjeh, S. Guha, C. Weedbrook, D. Vitali, J. H. Shapiro, and S. Pirandola, Microwave Quantum Illumination, Phys. Rev. Lett. 114, 080503 (2015).
- [58] E. D. Lopaeva, I. Berchera, I. P. Degiovanni, S. Olivares, G. Brida, and M. Genovese, Experimental Realization of Quantum Illumination, Phys. Rev. Lett. 110, 153603 (2013).

- [59] Z. Zhang, S. Mouradian, F. N. C. Wong, and J. H. Shapiro, Entanglement-Enhanced Sensing in a Lossy and Noisy Environment, Phys. Rev. Lett. 114, 110506 (2015).
- [60] S. Barzanjeh, S. Pirandola, D. Vitali, and J.M. Fink, Microwave quantum illumination using a digital receiver, Sci. Adv. 6, eabb0451 (2020).
- [61] J. H. Shapiro, Defeating passive eavesdropping with quantum illumination, Phys. Rev. A 80, 022320 (2009).
- [62] Z. Zhang, M. Tengner, T. Zhong, F. N. C. Wong, and J. H. Shapiro, Entanglement's Benefit Survives an Entanglement-Breaking Channel, Phys. Rev. Lett. 111, 010501 (2013).
- [63] J. H. Shapiro, Z. Zhang, and F. N. C. Wong, Secure communication via quantum illumination, Quantum Inf. Process. 13, 2171 (2014).
- [64] Q. Zhuang, Quantum-Enabled Communication without a Phase Reference, Phys. Rev. Lett. **126**, 060502 (2021).
- [65] H. Shi, M.-H. Hsieh, S. Guha, Z. Zhang, and Q. Zhuang, Entanglement-assisted capacity regions and protocol designs for quantum multiple-access channels, npj Quantum Inf. 7, 74 (2021).
- [66] Q. Zhuang, Z. Zhang, and J. H. Shapiro, Optimum Mixed-State Discrimination for Noisy Entanglement-Enhanced Sensing, Phys. Rev. Lett. 118, 040801 (2017).
- [67] S. Guha, Q. Zhuang, and B. Bash, Infinite-fold enhancement in communications capacity using pre-shared entanglement, arXiv:2001.03934.
- [68] J. H. Shapiro, D. M. Boroson, P. B. Dixon, M. E. Grein, and S. A. Hamilton, Quantum low probability of intercept, J. Opt. Soc. Am. B **36**, B41 (2019).
- [69] C. N. Gagatsos, B. A. Bash, A. Datta, Z. Zhang, and S. Guha, Covert sensing using floodlight illumination, Phys. Rev. A 99, 062321 (2019).
- [70] M. A. Taylor, J. Janousek, V. Daria, J. Knittel, B. Hage, H.-A. Bachor, and W. P. Bowen, Biological measurement beyond the quantum limit, Nat. Photonics 7, 229 (2013).